Journal of Materials Processing Technology 210 (2010) 858–867

Contents lists available at ScienceDirect

Journal of Materials Processing Technology

journal homepage: www.elsevier.com/locate/jmatprotec

Analysis for the wear resistance anisotropy of diamond cutting tools in theory and experiment

W.J. Zong[a,*], Z.Q. Li[a], T. Sun[a], D. Li[a], K. Cheng[a,b]

[a] Center for Precision Engineering, Harbin Institute of Technology, Harbin 150001, China
[b] School of Engineering and Design, Brunel University, Uxbridge, Middlesex UB8 3PH, UK

ARTICLE INFO

Article history:
Received 3 December 2009
Received in revised form 27 January 2010
Accepted 27 January 2010

Keywords:
Diamond cutting tool
Wear resistance
Theoretical prediction
Tensile strength

ABSTRACT

In this work, the dynamic micro-mechanical strengths of diamond crystal are deduced in theory, including the tensile, shearing and compressive strengths. The calculated results reveal that the dynamic micro-mechanical strengths have great anisotropy, but the tensile strengths are less than the shearing and compressive ones in any orientation of any plane. Subsequently, a novel evaluation factor is proposed, which integrates from the theoretical tensile strength in the orientation of flank face paralleling to the cutting direction and the theoretical tensile strength in the orientation of rake face paralleling to the chip flowing direction. And then as expected, the anisotropy of the resistance to wear of diamond cutting tools can be predicted exactly through comparing the evaluation factor. Theoretical analyses indicate the larger the evaluation factor, the greater the wear resistance of diamond cutting tool is. Finally, the cutting experiments are carried out on the (1 1 1) silicon wafers, and the sampled data are well consistent with the theoretical predictions, which validates that the proposed evaluation factor is suited for predicting the anisotropy of the resistance to wear of diamond cutting tools.

1. Introduction

Diamond turning has been considered as a promising technique and extensively applied in different industrial sectors due to the highest profile accuracy and perfect surface integrity as achieved (Yuan et al., 2003). Such favorable machining technology, however, is heavily dependent on the ultra-precision machine tool, super stable environment and the highly integrated cutting tool (Ikawa et al., 1991). That is to say, even if the machine tool and environment are quite stable, the successive wear of cutting tool also will significantly influence the finished profile accuracy and surface integrity and degrade the service performance of components gradually. Because of the affinity mentioned above, therefore, the investigations on tool wear involved in diamond turning are always the most attractive topics, such as tool wear mechanism, modeling on wear as well as the control strategies in response to the whole wearing process.

Encompassing the wearing mechanism, many theories had been proposed. For instance, Maekawa and Itoh focused on the friction in nano-scale machining using the molecular dynamics (MD) simulation. According to the simulation results, they considered the atomistic wear is caused by the repetition of inter-diffusion between the work and tool atoms and re-adhesion of the worn atoms to the tool (Maekawa and Itoh, 1995). Paul et al. (1996) claimed that the chemical wear of diamond tools is due to the presence of unpaired d electrons in the sample being machined. Cheng et al. (2003) employed the MD simulation and AFM experiments to investigate the wear mechanism of diamond cutting tools, and they validated the thermo-chemical wear is the basic wearing process in nanometric machining. Zhou et al. (2003) studied the tool wear pattern using SEM, and they concluded that the diamond crystal orientations and the cutting temperature, i.e. the cutting velocity, are the main reasons causing uneven wear along the cutting edge. Yan et al. (2003) observed the worn cutting edge, the finished surface and the cutting chips with SEM. And they found the wear on flank face is predominant. For the flank wear, the wearing fashions include the abrasion, adhesion, micro-chipping as well as the micro-fractures. Schmitt et al. (1999) put forward the oxide- and metal-transferred particles, graphitization and adhesion of these particles are the vital parameters affecting the tribological behaviour of diamond surface. Uemura (2004) concluded the wear of diamond tools mainly suffers from the graphitization and diffusion in cutting the ferrous metal. Shimada et al. (2000) discovered the crucial factor leading to tool wear in machining copper is the oxidization of diamond carbon atoms.

On the modeling of wear volume, some theoretical prediction models had been built up. In terms of the chemical wear mechanism, Paul et al. (1996) proposed an experiential formula

* Corresponding author at: P.O. Box 413, Harbin Institute of Technology, Xidazhi Street No. 92, Harbin, Heilongjiang 150001, China. Tel.: +86 451 86412924; fax: +86 0451 86415244.
E-mail addresses: zongwenjun@hit.edu.cn, zongwenjun@163.com (W.J. Zong).

0924-0136/$ – see front matter © 2010 Elsevier B.V. All rights reserved.
doi:10.1016/j.jmatprotec.2010.01.018

to calculate the reaction rate between diamond tool and different transition complex. Based on the physical diffusion between diamond tool and ferrous metals, Uemura (2004) deduced a quantitative equation to predict tool wear volume based on the Fick's law. Moreover, the empirical models extracted from the effects of processing parameters using the statistics means had been developed by Krulewich (1996) and Born and Goodman (2001). Likewise, in order to determine the effects of AFM tip wear on the sampling, Khurshudov et al. (1997) collected a lot of experimental results, and consequently they fitted the wear rates of diamond tip according to different soft materials as scanned.

On the control of tool wear, some effective methods had been put forward. For example, in order to suppress the diffusion wear of diamond tools in machining ferrous metals, Evans (1991) demonstrated that operating under low temperature ambient can decrease the diffusion rate of diamond carbon atoms. Moriwaki (1991) suggested that to employ the elliptic vibration shortens the contact time between diamond tool and work, and hence the diffusion volume is cut down. Moreover, spraying the carbon inclusion containing gas proposed by Casstevens (1983) or spraying the carbon inclusion containing coolant found by Paul et al. (1996) also can fulfill the object above. By this means, the carbon atoms in environment that substituting for the carbon atoms of diamond tool will diffuse into the metal bulk and saturate it. For the sake of reducing the oxidization wear, Shimada et al. (2000) performed the machining operations in the oxygen-free atmosphere. To be different, enriching the covalent bonds of the machining materials is an effective and promising solution to avoid the chemical reaction between diamond tool and the machining materials (Kohlscheen et al., 2002). In order to improve tool wear resistance, Yuan et al. (1992) selected the desirable rake and flank faces according to the different frictional behaviours of diamond crystal planes. Recently Uddin et al. (2004) confirmed again the orientations of diamond cutting tools have significant effects on the wear proof. Brinksmeier and Glaebe performed different cutting tests to verify the effectiveness of the proposed approaches above. They found turning at cryogenic temperature can reduce tool wear by at least one order of magnitude. And the ultrasonic vibration cutting or altering the chemical composition, i.e. enriching the covalent bonds of the topmost layer of the machining workpiece, can reduce tool wear by about two orders of magnitude (Brinksmeier and Glaebe, 2001, 2008).

Unfortunately, the interesting works as reviewed above either concentrated on the observed experiment phenomena originating from either the cutting tool or the machining material, or focused on the processing experiences. And up to now few attentions were paid to the theoretical analyses for tool wear resistance resulting from the intrinsic properties of diamond crystal. In this work, therefore, the micro-mechanical strengths of diamond crystal are deduced in different orientations and on different planes. As expected finally, the anisotropy of wear proof of diamond cutting tools will be predicted theoretically in terms of the micro-mechanical strengths.

2. Theoretical deductions

2.1. Brittle–ductile transition theory

In author's previous works, a theory about brittle–ductile transition was proposed to reveal the material removal mechanism of the lapped surface layer of diamond cutting tools polished with mechanical lapping (Zong et al., 2005). Fig. 1 is a schematic representation of the dynamic interaction between diamond cutting tool and diamond grit in mechanical lapping. P_r is the dynamic applied load on the grit, V_r is the lapping velocity, $2a$ is the characteristic

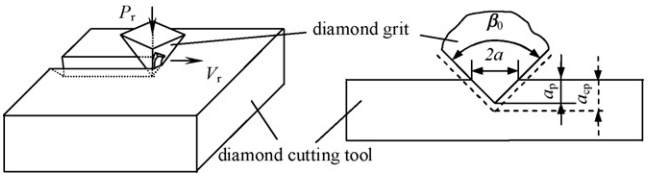

Fig. 1. Dynamic interaction between diamond grit and diamond cutting tool in mechanical lapping.

size of indentation, β_0 is the corner angle of grit, a_p is the dynamic depth of cut and a_{cp} is the critical depth of cut in lapping. So the dynamic applied load P_r is calculated as:

$$P_r = \frac{1}{2} \cdot P = \frac{1}{2} \cdot \alpha \cdot H \cdot a^2 \tag{1}$$

where P is the required load of indenter in Vickers indentation test, α is the geometrical factor of indenter, $\alpha = 1.8544$ and H, Knoop hardness in MPa.

As presented in Fig. 1, the geometrical relationship of $2a$, β_0 and a_p can be expressed:

$$2a = 2a_p \cdot \tan\left(\frac{\beta_0}{2}\right) \tag{2}$$

As it is known, the dynamic impact load P_{cd} in mechanical lapping is calculated as (Chen, 2001):

$$P_{cd} = \lambda_0 \cdot K_{Id} \cdot \left(\frac{K_{Id}}{H}\right)^3 \tag{3}$$

where λ_0 is the comprehensive coefficient, $\lambda_0 = (1.0–1.6) \times 10^4$, and K_{Id} is the dynamic fracture toughness property in MPa $m^{1/2}$.

Moreover, the fracture toughness property of a brittle material is dependent on the surface energy as required to create the full-fresh surfaces (Telling et al., 2000). And therefore, in terms of the relationship between K_{Id} and static fracture toughness property K_{Ic}, K_{Id} is given by (Field and Pickles, 1996)

$$K_{Id} = \frac{3 \cdot K_{Ic}}{10} = \frac{3 \cdot \sqrt{2\psi E\gamma}}{10} \tag{4}$$

where ψ is the coefficient depending on surface roughness and is assigned with 1.3 (ranging from 1 to 2) in present work, E is Young's modulus in MPa and γ is the surface energy required for fracture initiation in J m^{-2}.

According to the force balance between P_r and P_{cd} and the influence of orientations and crystal planes, the dynamic critical depth of cut a_{cp} for brittle–ductile transition of lapped tool surface layer is given by

$$a_{cp} = m_c \cdot m_o \cdot \cot\left(\frac{\beta_0}{2}\right) \cdot \sqrt{\frac{2\lambda_0}{\alpha}} \cdot \frac{9\psi E\gamma}{50H^2} \tag{5}$$

where m_c is the coefficient related to cleavage angle θ (the angle between lapped tool surface and cleavage plane), $m_c = \sin^2(\theta - 90^\circ)$. m_o is the coefficient depending on the orientation angle ω (the angle between lapping direction and the certain 'soft' direction) and characterizes with a symmetry. The (1 1 0) plane has a twofold symmetry, then $m_o^{(1\,1\,0)} = 9/35 + 5/35 \cdot \cos 2\omega$. The (1 0 0) plane has a fourfold symmetry, then $m_o^{(1\,0\,0)} = 7/18 + 3/18 \cdot \cos 4\omega$. And for the (1 1 1) plane, it has a threefold symmetry, therefore $m_o^{(1\,1\,1)} = 5/4 + 3/4 \cdot \cos 3\omega$.

The Young's modulus of crystal diamond has great anisotropy. The values of different crystal planes are: $E_{(1\,0\,0)} = 1050$ GPa, $E_{(1\,1\,0)} = 1165$ GPa and $E_{(1\,1\,1)} = 1207$ GPa (Telling et al., 2000). Also, the Knoop hardness has the same anisotropy, and it changes from 57 to 104 GPa. The order of the Knoop hardness among the three typical planes is that the (1 1 1) plane is the hardest, the (1 1 0) plane

is in the middle and the (1 0 0) plane is the softest. Corner angle β_0 is a given constant, i.e. 90° in this work. Fracture surface energy γ is 5.3 J m^{-2}. Cleavage angle, θ, is 144.73° of the (1 1 0) plane, 125.27° of the (1 0 0) plane and 109.5° of the (1 1 1) plane (Yuan et al., 2003).

2.2. Dynamic micro-mechanical strengths

At the present time, the popular method to evaluate micro-mechanical strength of diamond is the Hertzian indentation experiment (Ikawa et al., 1985). In the indentation test, the micro-tensile strength σ_t of diamond is given by (Field and Pickles, 1996)

$$\sigma_t = \frac{1-2\nu}{2p_c \sin^2(\theta - 90^\circ)} \tag{6}$$

where ν is Poisson's ratio of crystal diamond and p_c is the average compressive stress.

Like the calculation of average compressive stress in indentation tests, the same stress p_c' of diamond grit on diamond tool's surface in dynamic mechanical lapping is calculated as:

$$p_c' = \frac{P_r}{a^2} = \frac{P_r}{a_p^2 \tan^2(\beta_0/2)} \tag{7}$$

Combining the formulas from Eq. (1) to Eq. (7) and rearranging, the dynamic micro-tensile strength σ_{td} of single crystal diamond cutting tool is expressed as (Zong et al., 2007):

$$\sigma_{td} = m_d \cdot \frac{1-2\nu}{2} \cdot \frac{\lambda_0 \cdot K_{Id} \cdot (K_{Id}/H)^3}{a_{cp}^2 \cdot \tan^2(\beta_0/2)} \cdot \sin^2(\theta - 90^\circ)$$

$$= m_d \cdot \frac{81(1-2\nu) \cdot \lambda_0 \cdot (\psi E\gamma)^2 \cdot \sin^2(\theta - 90^o)}{5000 \cdot a_{cp}^2 \cdot H^3 \cdot \tan^2(\beta_0/2)} \tag{8}$$

where m_d is the correction coefficient due to the dynamic properties in lapping, m_d = 1/50.

The same as the calculations above, the dynamic micro-shearing strength τ_d of single crystal diamond cutting tool is calculated as:

$$\tau_d = m_d \cdot \frac{1-2\nu}{2} \cdot \frac{\lambda_0 \cdot K_{Id} \cdot (K_{Id}/H)^3}{a_{cp}^2 \cdot \tan^2(\beta_0/2)} \cdot \cos^2(\theta - 90^\circ)$$

$$= m_d \cdot \frac{81(1-2\nu) \cdot \lambda_0 \cdot (\psi E\gamma)^2 \cdot \cos^2(\theta - 90^\circ)}{5000 \cdot a_{cp}^2 \cdot H^3 \cdot \tan^2(\beta_0/2)} \tag{9}$$

Calculation of dynamic micro-compressive strength σ_{cd} of single crystal diamond cutting tool is different from that of σ_{td} and τ_d, and the cleavage angle should not be considered for it. Its calculating formula is given by

$$\sigma_{cd} = m_d \cdot \frac{1-2\nu}{2} \cdot \frac{\lambda_0 \cdot K_{Id} \cdot (K_{Id}/H)^3}{a_{cp}^2 \cdot \tan^2(\beta_0/2)}$$

$$= m_d \cdot \frac{81(1-2\nu) \cdot \lambda_0 \cdot (\psi E\gamma)^2}{5000 \cdot a_{cp}^2 \cdot H^3 \cdot \tan^2(\beta_0/2)} \tag{10}$$

The theoretical results of σ_{td}, τ_d and σ_{cd} on the three primary planes are presented in Fig. 2(a)–(c), respectively. As shown in these figures, the dynamic micro-mechanical strength σ_{td}, τ_d and σ_{cd} all have a visible anisotropy. For instance, the (1 1 0) plane presents a twofold symmetry, and the (1 0 0) plane shows a fourfold symmetry, while the (1 1 1) plane exhibits a threefold symmetry. Meanwhile in the 'soft' direction, the micro-tensile strength σ_{td} is 4.11 GPa of the (1 0 0) plane, 1.73 GPa of the (1 1 1) plane and 1.40 GPa of the (1 1 0) plane. The micro-shearing strength τ_d is 8.21 GPa of the (1 0 0) plane, 13.8 GPa of the (1 1 1) plane and 0.70 GPa of the (1 1 0) plane. For the micro-compressive strength, the (1 0 0) plane is 12.3 GPa, the (1 1 1) plane is 15.5 GPa and the (1 1 0) plane is 2.10 GPa. And in the 'hard' direction, the micro-tensile strength σ_{td} is 25.7 GPa of the (1 0 0) plane, 27.7 GPa of the (1 1 1) plane and 17.2 GPa of the (1 1 0) plane. The micro-shearing strength τ_d is 51.3 GPa of the (1 0 0) plane, 221.0 GPa of the (1 1 1)

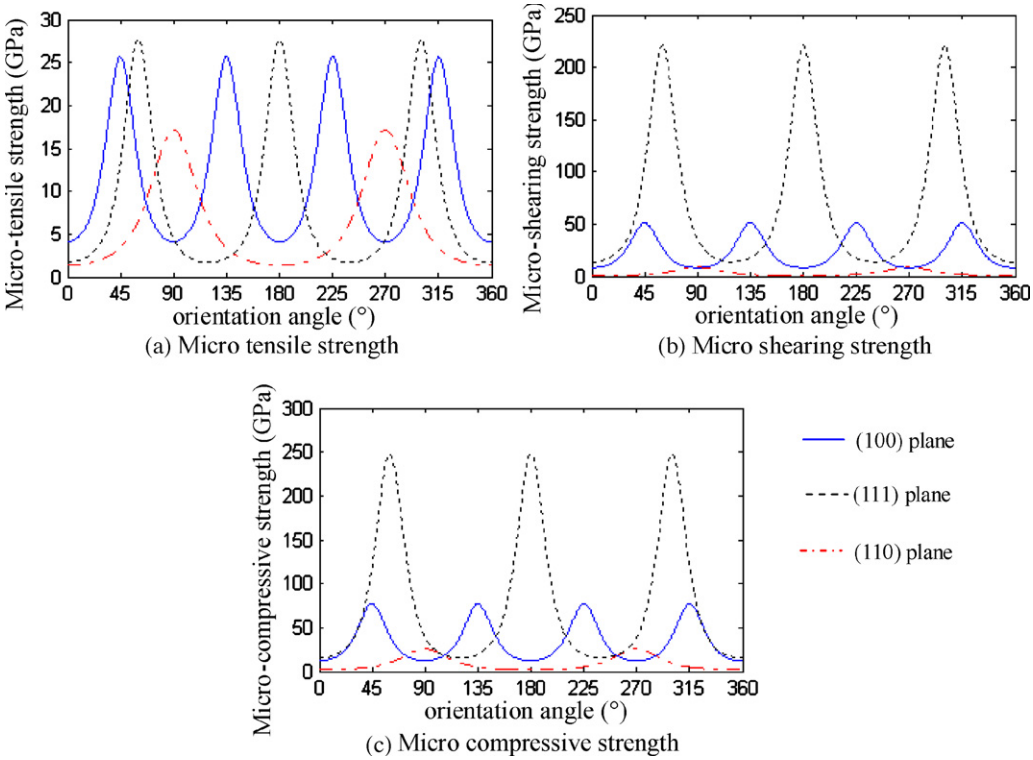

Fig. 2. Dynamic micro-mechanical strengths of single crystal diamond in different orientations and on different planes. (a) Micro-tensile strength, (b) micro-shearing strength, and (c) micro-compressive strength.

Table 1
Micro-strengths in the 'soft' and 'hard' directions of the three typical planes [GPa].

	'Soft' direction			'Hard' direction		
	Tensile	Shearing	Compressive	Tensile	Shearing	Compressive
(1 1 0)	1.40	0.70	2.10	17.2	8.59	25.8
(1 0 0)	4.11	8.21	12.3	25.7	51.3	77.0
(1 1 1)	1.73	13.8	15.5	27.7	221.0	248.7

plane and 8.59 GPa of the (1 1 0) plane. The micro-compressive strength is 77.0 GPa of the (1 0 0) plane, 248.7 GPa of the (1 1 1) plane and 25.8 GPa of the (1 1 0) plane. The data calculated above are listed in Table 1.

Comparing the data listed in Table 1 gives an indication that the dynamic micro-mechanical strength in the 'soft' direction is less than that in the 'hard' direction. And in the identical orientation, except for the (1 1 0) plane, the dynamic micro-compressive and shearing strengths are both larger than the micro-tensile strength on the (1 0 0) and (1 1 1) planes. That is to say, the resistance to tension of diamond crystal is relatively poor. In present work, therefore, the tensile strength is employed to predict the anisotropy of wear resistance of diamond cutting tool.

2.3. Predictions of wear resistance

In order to present a distinct analysis for the anisotropy of wear resistance, four diamond cutting tools were designed, which had different combinations in the orientation on the rake and flank faces. The design details can be found in Fig. 3, where 'R' and 'F' denote the rake face and flank face, (1 0 0) and (1 1 0) denote the (1 0 0) plane and (1 1 0) plane of diamond crystal.

As is known, a super-smooth mirror surface can be achieved directly by using of diamond turning process as long as the unwanted surface layer is removed in ductile mode, regardless of the plasticity or ductility of the machined workpiece. In return however, the ductile removal leads to the unavoidable wearing of diamond cutting tool more or less, such as the abrasion, adhesion, diffusion, oxidation as well as the groove marks. Analyzing from the microscopic viewpoint, the successive breakage of C–C covalent bond on the topmost layer of cutting edge is necessary while diamond tool suffers from those wearing processes. Obviously, the difficulty in breakage is decided by the tensile strength of C–C bond. In other words, the greater the tensile strength of C–C bond is, the harder the appearance of the breaking of C–C bond, and resultantly the stronger the wear resistance. On the other side in the SPDT (single point diamond turning) operations, the noticeable cutting forces are the tangential force and the thrust force, which are parallel to the cutting direction and the chip flowing direction respectively as shown in Fig. 3. This means the breakage of C–C bond on the cutting edge is dependent on the tensile strengths of both flank face and rake face. And hence, the idea to compose the tensile strengths of flank face and rake face is introduced in this work. Additionally, the visible wear generally takes place on tool flank face due to the severer contact condition than that upon the rake face in the SPDT operations. And hence, more attention should be paid to the tensile strength of flank face along the cutting direction. In order to compare the wear resistance exactly, therefore, a novel evaluation factor is proposed in this work for the first time, in which a bigger calculation weight is given to the tensile strength of flank face. The evaluation factor, A_e, is calculated as:

$$A_e = \sqrt{\sigma_{td-f}^2 + \sigma_{td-r}^2 \cdot W_{td-r}} \tag{11a}$$

where σ_{td-f} is the tensile strength of flank face along the cutting direction, σ_{td-r} is the tensile strength of rake face along the chip flowing direction, and W_{td-r} is a weighting factor of $\sigma_{td-r} < 1.0$.

The results presented later suggest empirically that the following value of W_{td-r} results in a good correlation between A_e and wear resistance, which is given by

$$W_{td-r} = \left[\frac{\sigma_{td-f} \cdot \sigma_{td-r}}{\max(\sigma_{td-f}^2, \sigma_{td-r}^2)} \right]^{3/2} \tag{11b}$$

Seeing from Fig. 3(a), the cutting direction of the R(1 0 0)F(1 0 0) oriented tool is parallel to the 'soft' direction of flank face, i.e. the (1 0 0) plane, and the chip flowing direction is also parallel to the 'soft' direction of rake face or the (1 0 0) plane. And so it can be known the σ_{td-f} and σ_{td-r} are both 4.11 GPa. Substituting for σ_{td-f} and σ_{td-r} into Eq. (11) gives 5.81 GPa to A_e. For the R(1 0 0)F(1 1 0) oriented tool, the cutting direction is just parallel to the 'soft' direction of the (1 1 0) plane, and the chip flowing direction is parallel to the 'hard' direction of the (1 0 0) plane, as graphically presented in Fig. 3(b). Substituting for the related σ_{td-f} and σ_{td-r} into Eq. (11) outputs 3.22 GPa for A_e. And as exhibited in Fig. 3(c), the cutting direction of the R(1 1 0)F(1 0 0) oriented tool is parallel to the 'hard' direction of the (1 0 0) plane, but the chip flowing direction is parallel to the 'soft' direction of the (1 1 0) plane. And then substituting for the corresponding σ_{td-f} and σ_{td-r} into Eq. (11) configures A_e as 25.7 GPa. Likewise, the pictorial presentation of Fig. 3(d) inform that the cutting direction and the chip flowing direction of the R(1 1 0)F(1 1 0) oriented tool are both parallel to the 'hard' direction of the (1 1 0) plane. This means its σ_{td-f} and σ_{td-r} are both 17.2 GPa, and the resultant A_e is 24.3 GPa. All the calculated evaluation factors of these four designed tools are listed in Table 2.

Comparing the evaluation factors in Table 2, it can be found the largest is the R(1 1 0)F(1 0 0) oriented tool, the second of the R(1 1 0)F(1 1 0), the third of the R(1 0 0)F(1 0 0) and the smallest of the R(1 0 0)F(1 1 0) oriented one. Such ranking order implies that the R(1 1 0)F(1 0 0) oriented tool can provide with the most excellent wear resistance, and the R(1 0 0)F(1 1 0) orientated tool has the worst resistance, while the R(1 0 0)F(1 1 0) and R(1 0 0)F(1 0 0) oriented tools rank the second and the third, respectively. Furthermore, the minute difference in the values of the R(1 1 0)F(1 0 0) and R(1 1 0)F(1 1 0) oriented tools A_e indicate they have the approximate proof to wear. Likewise, the wear performance of the R(1 0 0)F(1 0 0) oriented tool is approximate to the R(1 0 0)F(1 1 0) oriented tool's.

3. Experimental validations

3.1. Ultra-precision machine tool

A home-made T-type ultra-precision machine tool was employed for the cutting tests. Fig. 4 is a close-up of this experiment setup. As shown in this picture, in order to obtain a damage-free silicon surface, the air-bearing spindle with high running accuracy and high stiffness had been integrated into this setup, i.e. 567 N/μm

Table 2
Evaluation factors of four designed diamond cutting tools [GPa].

	R(1 0 0)F(1 0 0)	R(1 0 0)F(1 1 0)	R(1 1 0)F(1 0 0)	R(1 1 0)F(1 1 0)
Ae	5.81	3.22	25.7	24.3

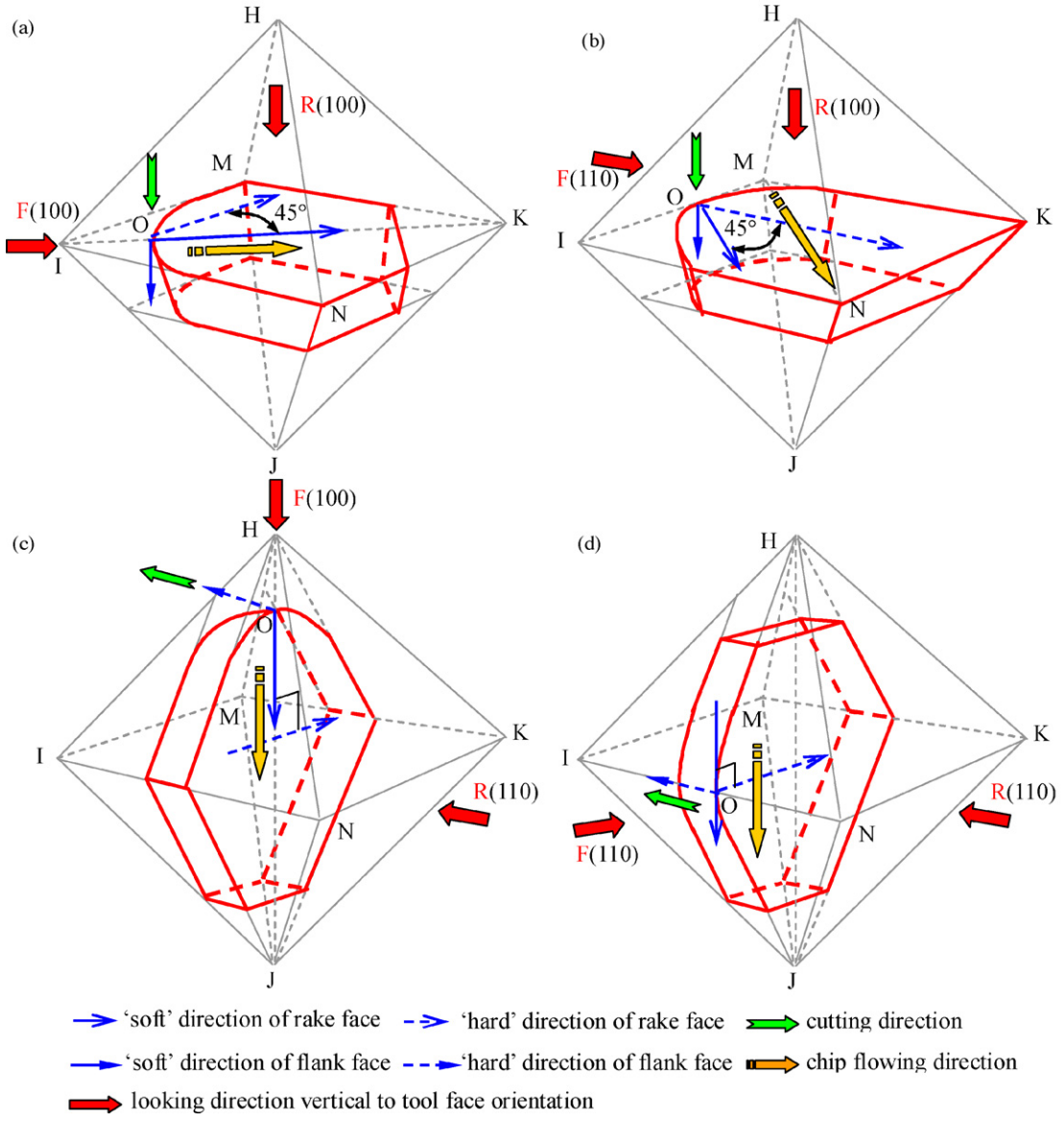

Fig. 3. Schematic diagram of diamond cutting tools with different orientations on rake and flank faces: (a) R(1 0 0)F(1 0 0), (b) R(1 0 0)F(1 1 0), (c) R(1 1 0)F(1 0 0), and (d) R(1 1 0)F(1 1 0).

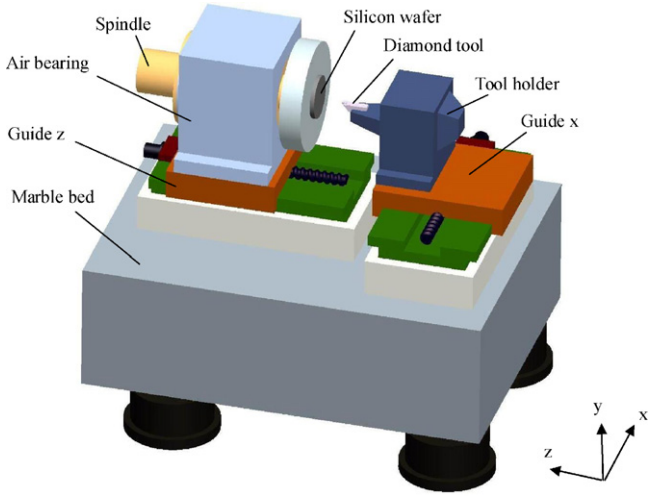

Fig. 4. Schematic illustration of the ultra-precision machine tool.

in radial direction and 450 N/μm in axial direction with a running accuracy of less than 50 nm. The long-range moving resolutions of guides *x* and *z* are both 100 nm.

3.2. Workpiece and diamond cutting tools

Monocrystalline silicon (1 1 1) wafers were employed as the workpiece because such material can result in the heavy wear on tool so as to shorten the whole test time. Additionally, the radial size of any silicon wafer is identical, i.e. that 17.6 mm in outer radius and 7.4 mm in inner radius with a thickness of 0.5 mm. In order to prepare the smooth surfaces used in the wear cutting tests, the silicon wafers were initially processed with some pristine diamond cutting tools, rather than the designed four cutting tools. Moreover, the tools to smoothen the silicon surfaces before the wear tests would be polished frequently to ensure a sharpened cutting edge. Subsequently four designed diamond cutting tools with different orientations were installed to perform the wearing experiments. The detailed orientations can be found in Fig. 3. Moreover, four designed cutting tools all have a nose radius of 5 mm, a rake angle

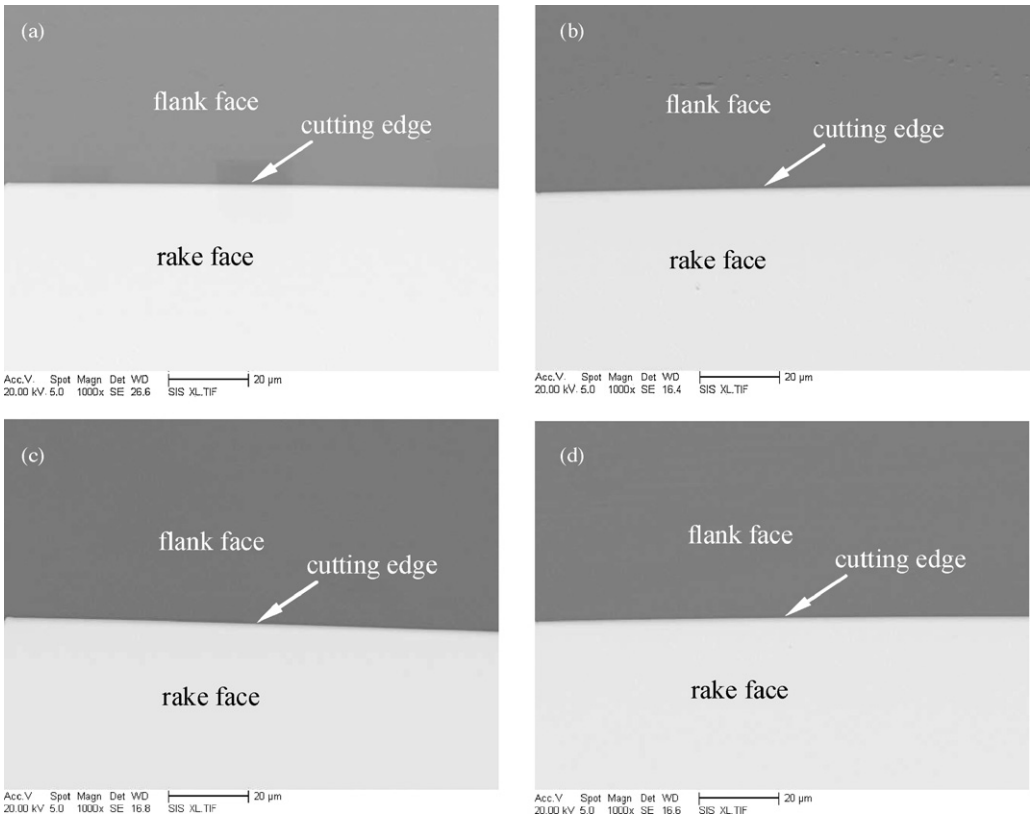

Fig. 5. SEM topographies of the initial cutting edges of four tested tools: (a) R(1 0 0)F(1 0 0), (b) R(1 0 0)F(1 1 0), (c) R(1 1 0)F(1 0 0), and (d) R(1 1 0)F(1 1 0).

of 0° and a clearance angle of 6°. The SEM topographies of the full-fresh cutting edges of these four tools are presented in Fig. 5.

3.3. Cutting parameters

As shown in Fig. 4, the facing operation was carried out and no coolant was used in this work. In order to obtain the mirror-like surface by facing, the selection of cutting parameters should meet the requirement of the ductile removal process. The finally designed configurations of all cutting parameters are listed in Table 3. As well known, the actual removal mode of the silicon surface in facing is restricted by the maximal undeformed chip thickness d_{max}. For a rounded diamond cutting tool, the maximal undeformed chip thickness d_{max} is calculated as (Uddin et al., 2004):

$$d_{max} = R_\varepsilon - \sqrt{R_\varepsilon^2 + f^2 - 2f\sqrt{2R_\varepsilon a_p - a_p^2}} \quad (12)$$

where R_ε is the tool nose radius, f the feed rate and a_p the depth of cut.

Substituting for the related cutting parameters into Eq. (12) gives a value of 15.6 nm to d_{max}. Whereas the minimal critical cutting thickness of the (1 1 1) silicon wafer for ductile–brittle transition is 92 nm (Yan et al., 2003), which is much more than the d_{max} as calculated in this work. That is to say, the facing operations of this work were all in ductile mode.

Moreover, when the diamond cutting tool fulfills one-run facing operation, the individual cutting distance, L, is given by

$$L = \frac{\pi(r_{out}^2 - r_{in}^2)}{f} \quad (13)$$

where r_{out} and r_{in} are the outer radius and inner radius of silicon wafer, respectively. In this work, r_{out} is 17.6 mm and r_{in} is 7.4 mm.

Table 3
Specifications of cutting parameters.

Cutting parameter	Configuration
Spindle speed [rpm]	800
Cutting velocity [m/s]	0.62–1.47
Depth of cut [μm]	1.5
Feed rate [μm/r]	0.64
Undeformed chip thickness [nm]	15.6
One-run cutting distance [km]	1.25

4. Results and discussions

4.1. Surface roughness

The surface roughness of the machined silicon wafers was appraised by AFM, and the scanning scope is 40 μm × 40 μm. In advance of scanning, the finished surfaces were all cleaned in acetone aided with ultrasonic. Fig. 6 shows the sampled data achieved at different cutting distance. It can be seen clearly in this view the surface roughness Ra (average roughness) and Rms (root mean square roughness) generated by any cutting tool degrade with the increment of cutting distance. This is because while the cutting distance advances, the tool wear grows up too. And the increment of tool wear leads to the enlarging of cutting edge radius finally. As well known in diamond turning of silicon wafer, an extremely sharpened cutting edge is the quite necessary condition for finishing a mirror-like surface through ductile removing the unwanted surface layer. Therefore, while the cutting edge becomes blunt gradually, the brittle fracture will account for the primary removal mode step by step, which generates the worsening surface roughness. For instance for the R(1 0 0)F(1 0 0) oriented tool, the achieved surface roughness is 3.9 nm in Ra and 4.7 nm in Rms after the first run facing, but 36.5 nm in Ra and 67.2 nm in Rms after the last run

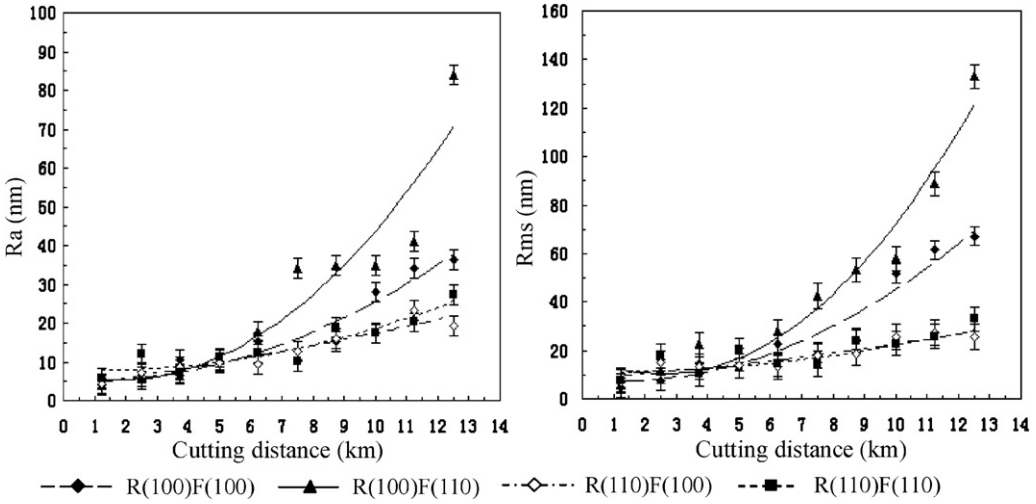

Fig. 6. Relationship of the achieved surface roughness versus cutting distance.

facing, as compared in Fig. 7. Furthermore, the curves fluctuation in Fig. 6 demonstrates the surface roughness achieved by these four tools have no visible differences while the cutting distance is less than 4.5 km, all being less than 10 nm in Ra or 15 nm in Rms. But the considerable anisotropy appears once the cutting distance goes beyond 4.5 km. Seeing clearly from Fig. 6, the R(1 0 0)F(1 1 0) oriented tool produces the worst surface roughness, and the best of the R(1 1 0)F(1 0 0) and R(1 1 0)F(1 1 0) oriented tools because they finish almost the same roughness. In return, therefore, the wear resistance of these four tested tools can be inferred in terms of the anisotropy of the surface roughness, i.e. that the R(1 1 0)F(1 0 0) and R(1 1 0)F(1 1 0) oriented tools are the strongest, the second of the R(1 0 0)F(1 0 0) oriented tool and the worst of the R(1 0 0)F(1 1 0) oriented tool. To be apparent, such order is consistent with the theoretical prediction.

4.2. Height and width of wear band

The wear band height and width on flank face of these four tested tools after any run facing were measured with the optical microscope and SEM. It should be noted the wear band width is the wear dimension along the cutting edge, and the wear band height is the wear dimension perpendicular to the cutting edge. All the collected results are presented in Fig. 8. As shown in this map, the height and width of wear band of four tools grow up with the advance in cutting distance, which means the wear volumes of four tested tools aggravate gradually. Moreover, it can be seen clearly from Fig. 8(a) the wear height exhibits an evident difference, i.e. the R(1 0 0)F(1 0 0) oriented tool ranks the smallest, the second of R(1 1 0)F(1 0 0), the third of R(1 1 0)F(1 1 0) and the largest of R(1 0 0)F(1 1 0). Furthermore, according to the variations in wear width as shown in Fig. 8(b), the visible anisotropy also can be found among these four tested cutting tools, e.g. the R(1 1 0)F(1 0 0) oriented tool has the smallest width after any run facing, the second and the third are the R(1 1 0)F(1 1 0) and R(1 0 0)F(1 0 0) oriented tools, while the R(1 0 0)F(1 1 0) oriented tool creates the largest width. Obviously, the wear proof of these four tools can be classified directly by referring to the variations in the wear band height and width versus the cutting distance. As the presented case of this work, the arrangement of the wear band height or width basically agrees with the predicted anisotropy.

4.3. Cutting forces

In this work, the tangential and thrust cutting forces at any run facing were recorded using Kistler 3-Components precision dynamometer 9256A1. Fig. 9 represents all the sampled data. As shown in this view, the tangential force and the thrust force both enlarge with the advance of cutting distance, i.e. the increment of wearing volume. The anisotropy of tool wear resistance, however,

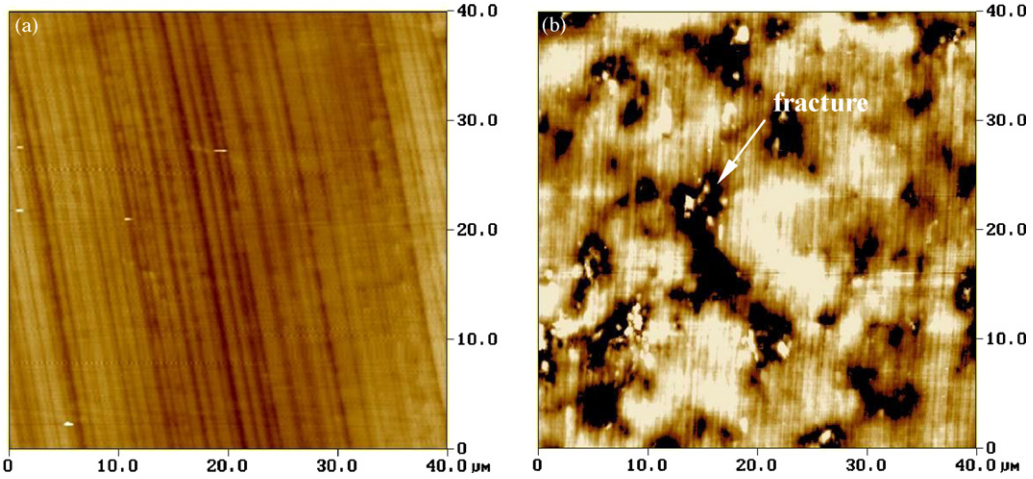

Fig. 7. AFM scanned surface topographies achieved by the R(1 0 0)F(1 0 0) oriented tool at different cutting distance: (a) 1.25 km and (b) 12.5 km.

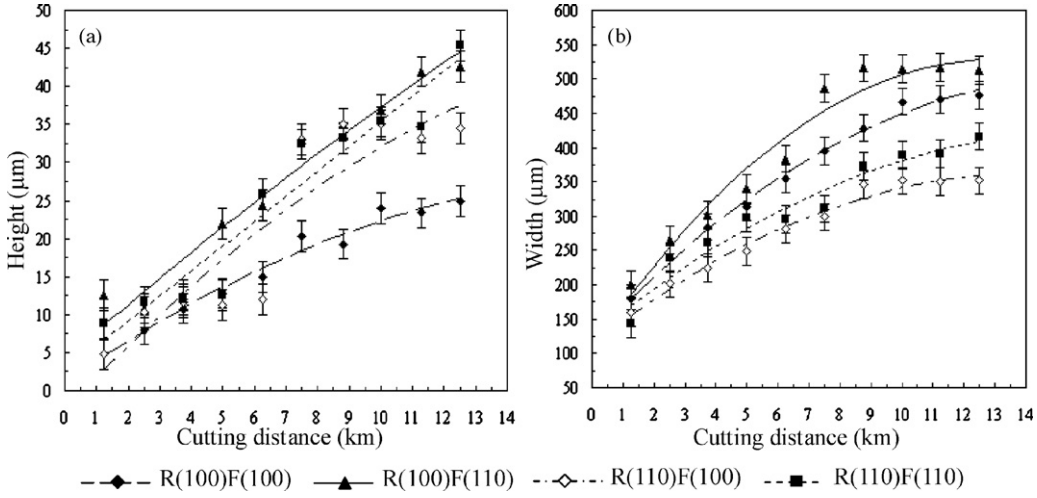

Fig. 8. Relationship of wearing band height and width versus cutting distance.

can not be distinguished simply in terms of the variations of cutting force. This is because the cutting forces are heavily dependent upon the orientations of the rake and flank faces, even though the tool wear has an important influence on the cutting forces. For the diamond crystal as known, different crystal plane presents different frictional coefficient in contacting with the other materials. In practice, the (1 1 0) plane provides with a bigger frictional coefficient than the (1 0 0) plane. Therefore, the tested tools having a (1 1 0) plane on the flank face output a relatively large tangential cutting force, and the tested tools having a (1 0 0) plane on the rake face generate a smaller thrust cutting force. Apparently, such explanation accords with the variation of the force curves as exhibited in Fig. 9.

In order to make an exact identification in the wear resistance anisotropy of these four tested tools, the force ratio of thrust force to tangential force at any run facing is calculated. Subsequently, the wear resistance anisotropy will be deduced by inspecting the stability of the force ratio. The central idea of this solution is that the stabler the force ratio is, the better the wear resistance of the cutting tool. The finally calculated results are demonstrated in Fig. 10. In this figure, the force ratios generated by the R(1 0 0)F(1 0 0) and R(1 0 0)F(1 1 0) oriented tools are unstable due to the declining tendency of the former and the ascending tendency of the latter. To be different, however, the force ratio fluctuations resulted from the R(1 1 0)F(1 0 0) and R(1 1 0)F(1 1 0) oriented tools are relatively small. The force ratios of these two tools level off quickly at the followed facing although they both climb up at the initial stage. According to the analyses above, therefore, it can be concluded that the R(1 1 0)F(1 0 0) and R(1 1 0)F(1 1 0) oriented tools have much stronger wear resistance than the left two tools. This result agrees with the theoretical predictions too.

4.4. Diffusion of diamond carbon

Yan et al. (2003) considered that the diffusion of diamond carbons is one possible wearing fashion in terms of the experimental observations. Recently Cheng et al. (2003) confirmed the presence of diffusion of diamond carbon atoms in diamond turning with the molecular dynamics simulation. And therefore in this work, in order to distinguish the wear resistance of these four tested tools, a qualitative analysis for the carbon concentration on the topmost surface layer of the machined silicon wafer was carried out resorting to the X-ray photoelectron spectroscopy (XPS) technology. Before XPS sampling, all the faced silicon surfaces were cleaned with acetone. And subsequently the inspected points were sputtered with argon ions for 480 s. Such arrangement was meant to avoid the disturbance of the pollution carbon as possible. Table 4 shows a collected atomic concentration of the topmost silicon surface machined with the R(1 1 0)F(1 0 0) oriented tool after one-run facing. Seeing from this table, considering that the inspected point was pre-sputtered

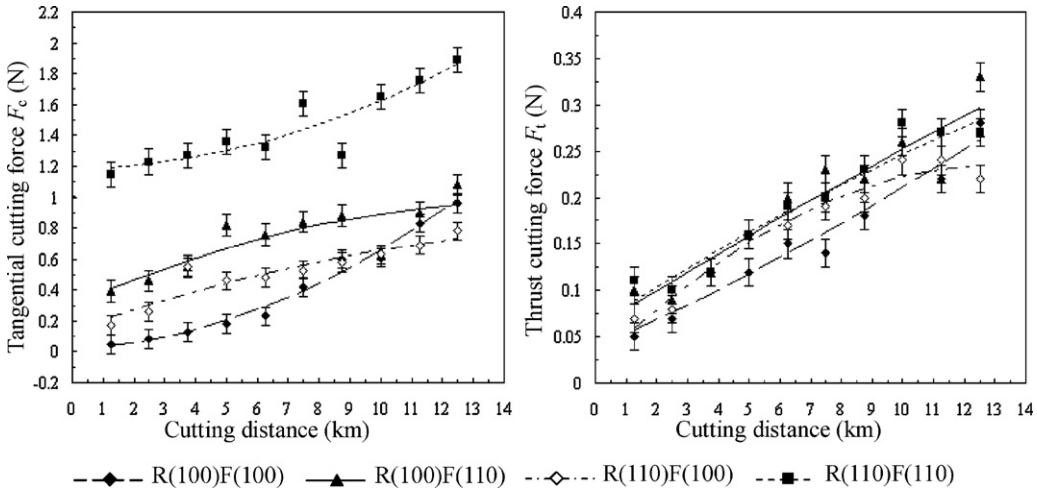

Fig. 9. Relationship of dynamic micro-cutting forces versus cutting distance.

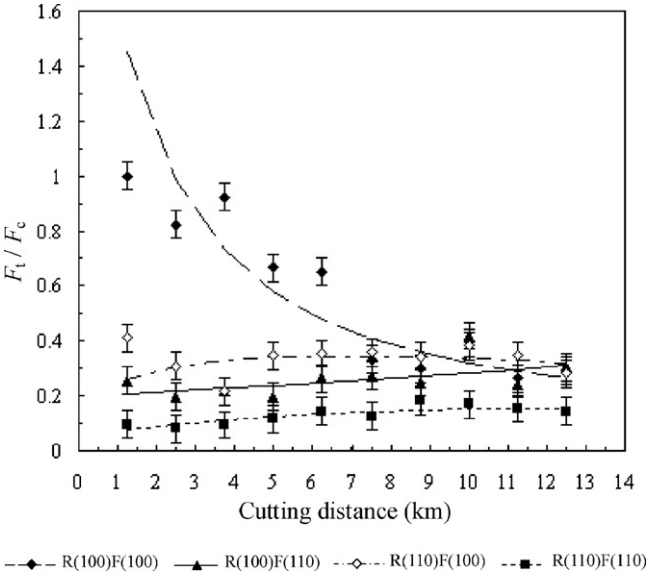

Fig. 10. Relationship of cutting force ratio versus cutting distance.

Table 4
Atomic concentration of the topmost silicon surface machined with the R(1 1 0)F(1 0 0) oriented tool after one-run facing.

Element	Concentration [%]
C	12.54
O	11.51
Si	71.47
Ar	4.48

with argon ions, therefore the collected data has an atomic concentration of 4.48% for the polluted element Ar.

The collected values of the carbon concentration are all plotted in Fig. 11. It can be seen a lot of scatter exists in the sampled data, which seems that the tool wear process goes in pulses, rather than at a constant rate. The data scatter appearing in this figure mainly comes from two reasons. One is the size effect. For the sake of obtaining the mirror-like silicon surface, the maximal undeformed chip thickness is only 15.6 nm in this work. In nanometric cutting the great variation in the carbon concentration is unavoidable. The other is the metrology method. As well known, XPS is only suited for the qualitative analysis on the chemical composition. For the quantitative comparison of the concentration of a certain chemical element, the great variation in the sampled data is inevitable too. And therefore a statistical solution, i.e. the least squares linear fit, is employed to overcome the data scatter in this work. As shown in Fig. 11, the intersected values of the R(1 1 0)F(1 0 0) and R(1 1 0)F(1 1 0) oriented tools between the fitted line and the longitudinal coordinate, i.e. the carbon concentration bar, are about 13.2% and 13.5%, but 16.7% and 17.4% of the R(1 0 0)F(1 0 0) and R(1 0 0)F(1 1 0) oriented tools. Moreover, the declining rates of the former two tools are obviously smaller than the latter two tools. As a precursory condition, the diamond carbon atoms must depart from the cell of diamond crystal before they diffuse into the machined silicon surface. And therefore, the phenomena as revealed in Fig. 11 demonstrate that the breakage of C–C covalent bond on the cutting edge of the former two tools is more difficult than the latter two tools. In conclusion, viewing from the resistance to diamond carbon diffusion, the tools oriented as R(1 1 0)F(1 0 0) and R(1 1 0)F(1 1 0) have more excellent wear proof than the R(1 0 0)F(1 0 0) and R(1 0 0)F(1 1 0) oriented tools, which confirms again that the theoretical prediction is effective and can be applied in the industrial production.

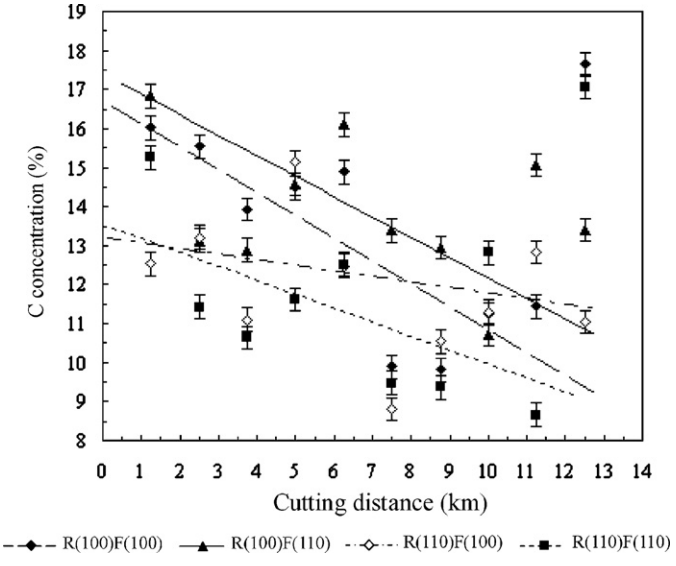

Fig. 11. Carbon concentration variation induced by diamond cutting tool's orientations.

On the other side, the declining tendencies of these four tested tools show that the carbon diffusion weakens with an increment in cutting distance. Such variation can be explained that when the tool wear accumulates along with the increase of cutting distance, the successively blunted cutting edge can not keep up the ductile facing at all times. And therefore the primary removal mode of the faced silicon surface transfers from the ductile manner to the brittle manner gradually, as compared in Fig. 7. As a result, the increment of brittle removals leads to more and more unpleasant chatters between the machining wafer surface and diamond cutting tool, which will frequently interrupt the diffusion process of diamond carbons in return. Consequently, the diamond carbons diffusing into the machined silicon surface decrease.

5. Conclusions

In this work, the dynamic micro-mechanical strengths of diamond crystal are calculated firstly. In order to predict the wear resistance of diamond cutting tools subsequently, a novel evaluation factor is proposed, which integrates from the tensile strength in the orientation of flank face paralleling to the cutting direction and the tensile strength in the orientation of rake face paralleling to the chip flowing direction. In terms of the theoretical deduction and the appended experimental validation, some significant conclusions can be drawn as follows:

(1) The dynamic micro-tensile, shearing and compressive strengths all have visible anisotropy. However, the tensile strength is less than the compressive and shearing ones in any orientations of any crystal planes.
(2) The greater the evaluation factor is, the finer the wear resistance of diamond cutting tool.

Acknowledgements

The Authors would thank the Natural Science Foundation of China (Contract No. 50705025) and the 111 Project of the Ministry of Education of China (Contract No. B07018) for the supports of this work. Furthermore, the authors would sincerely thank the reviewers for their very professional suggestions on this work.

References

Born, D.K., Goodman, W.A., 2001. An empirical survey on the influence of machining parameters on tool wear in diamond turning of large single-crystal silicon optics. Precision Engineering 25, 247–257.

Brinksmeier, E., Glaebe, R., 2001. Advance in precision machining of steel. Annals of the CIRP 50 (1), 385–388.

Brinksmeier, E., Glaebe, R., 2008. Diamond Machining of Steel Molds for Optical Applications. Key Engineering Materials 364–366, 701–706.

Casstevens, J., 1983. Diamond turning of steel in carbon saturated environments. Precision Engineering 5, 9–15.

Chen M J, 2001. Research on ultra-precision aspheric surface grinding technique. Ph.D. Dissertation. Harbin Institute of Technology, pp. 54–56.

Cheng, K., Luo, X., Ward, R., Holt, R., 2003. Modeling and simulation of the tool wear in nanometric cutting. Wear 255, 1427–1432.

Evans, C.J., 1991. Cryogenic diamond turning of stainless steel. Annals of the CIRP 40 (1), 571–575.

Field, J.E., Pickles, C.S.J., 1996. Strength, fracture and friction properties of diamond. Diamond and Related Materials 5, 625–634.

Ikawa, N., Shimada, S., Tsuwa, H., 1985. Non-destructive strength evaluation of diamond for ultra-precision cutting tool. Annals of the CIRP 34 (1), 117–120.

Ikawa, N., Donaldson, N.N., Komanduri, R., Koenig, W., Aachen, T.H., Mckeown, P.A., Moriwaki, T., Stowers, I.F., 1991. Ultra-precision metal cutting-the past, the present and the future. Annals of the CIRP 40 (2), 587–594.

Krulewich, D.A., 1996. Experimental Design for Single Point Diamond Turning of Silicon Optics, UCRL-ID-127385.

Khurshudov, A.G., Kato, K., Koide, H., 1997. Wear of the AFM diamond tip sliding against silicon. Wear 203–204, 22–27.

Kohlscheen, J., Stock, H.-R, Mayr, P., 2002. Tailoring of diamond machinable coating materials. Precision Engineering 26, 175–182.

Maekawa, K., Itoh, A., 1995. Friction and tool wear in nano-scale machining-a molecular dynamics approach. Wear 188, 115–122.

Moriwaki, T., 1991. Ultraprecision diamond turning of stainless steel by applying ultrasonic vibration. Annals of the CIRP 40 (1), 559–562.

Paul, E.D., Evans, C.J., Mangamelli, A., McGlauflin, M.L., Polvanit, R.S., 1996. Chemical aspects of tool wear in single point diamond turning. Precision Engineering 18, 4–19.

Schmitt, M., Paulmier, D., Huu, T.L., 1999. Influence of diamond crystal orientation on their tribological behaviour under various environments. Thin Solid Films 343–344, 226–229.

Shimada, S., Lnamura, T., Higuchi, M., Tanaka, H., Ikawa, N., 2000. Suppression of tool wear in diamond turning of copper under reduced oxygen atmosphere. Annals of the CIRP 49 (1), 21–24.

Telling, R.H., Pickard, C.J., Payne, M.C., Field, J.E., 2000. Theoretical strength and cleavage of diamond. Physical Review Letters 84 (22), 5160–5163.

Uddin, M.S., Seah, K.H.W., Li, X.P., Rahman, M., Liu, K., 2004. Effect of crystallographic orientation on wear of diamond tools for nano-scale ductile cutting of silicon. Wear 257, 751–759.

Uemura, M., 2004. An analysis of the catalysis of Fe, Ni or Co on the wear of diamonds. Tribology International 37, 887–892.

Yan, J.W., Syoji, K., Tamaki, J., 2003. Some observations on the wear of diamond tools in ultra-precision cutting of single-crystal silicon. Wear 255, 1380–1387.

Yuan, Z.J., He, J.C., Yao, Y.X., 1992. The optimum crystal plane of natural diamond tool for precision machining. Annals of the CIRP 41 (1), 605–608.

Yuan, Z.J., Yao, Y.X., Zhou, M., Bai, Q.S., 2003. Lapping of single crystal diamond tools. Annals of the CIRP 52 (1), 285–288.

Zhou, M., Ngoi, B.K.A., Wang, X.J., 2003. Tool wear in ultra-precision diamond cutting of non-ferrous metals with a round-nose tool. Tribology Letters 15, 211–216.

Zong, W.J., Cheng, K., Li, D., Sun, T., Liang, Y.C., 2007. The ultimate sharpness of single crystal diamond cutting tools. Part I. Theoretical analyses and predictions. International Journal of Machine Tools & Manufacture 47 (5), 852–863.

Zong, W.J., Li, D., Cheng, K., Sun, T., 2005. The material removal mechanism in mechanical lapping of diamond cutting tools. International Journal of Machine Tools & Manufacture 45 (7–8), 783–788.